

Supporting information

**Bismuth/Tin-based artificial interface for overcoming the anode
passivation of rechargeable magnesium batteries**

Xiaolong Hou ^a, Jingfei Guan ^a, Baifei Wu ^b, Caini Yi ^a, Shuo Wang ^a, Guimiao Wang ^a, Hang Yang ^a,
Min Liu ^a, Meilin Chen ^a, Danmei Yu ^a, * Liyong Gan ^b, Xiaoyuan Zhou ^b, *

^a School of Chemistry and Chemical Engineering, Chongqing University, Chongqing 401331, P.R.
China

^b College of Physics, Chongqing University, Chongqing, 401331, P.R. China

*Corresponding authors

Danmei Yu's e-mail: yudanmei-1@163.com.

Xiaoyuan Zhou's e-mail: xiaoyuan2013@cqu.edu.cn.

Experimental Section

Experimental material

1,2-Dimethoxyethane (DME), BiCl_3 and SnCl_2 (AR, 99%) were received from Shanghai Macklin Biochemical Technology Co., Ltd., Mg foil was purchased from North China Mg Processing Plant. The electrolyte was provided by Suzhou Duoduo Chemical Technology Co., Ltd., in which the solvent was DME, and the solutes were $\text{Mg}(\text{TFSI})_2$ (0.5 M $\text{Mg}(\text{TFSI})_2$ in DME=100 Vol%). The glass fiber separator (GF/A, Whatman) purchased from Shanghai Jinpan Biotechnology Co., Ltd. Molybdenum sulfide (Mo_6S_8) was synthesized by oneself in laboratory.

Synthesis of artificial interface layer

The synthesis process of artificial interface was conducted in an argon-filled glovebox, with oxygen and moisture levels maintained at less than 0.1 ppm. At first, Mg metal foils were thoroughly polished with sandpaper to remove oxide artificial interface and expose fresh surface, and then punched into the disks with a diameter of 14 mm. Subsequently, the prepared Mg disks in advance were immersed into the solution containing concentrations of 0.1 M BiCl_3 and 0.1 M SnCl_2 with DME. After that, the surface of Mg foil disks gradually turned black and then we washed them repeatedly with DME several times to eliminate any residual reactants. These treated Mg foil disks were abbreviated as BiSn@Mg, which were carefully transferred into a holder and then dried for 3 hours in the glovebox before being used. For comparison, Bi@Mg was also prepared in the DME solution only containing 0.1 M BiCl_3 while Sn@Mg was obtained from the solution of 0.1 M SnCl_2 with DME.

Cell assembly

The entire assembly process of half-cells, symmetrical cells and full-cells is carried out in an argon-filled glovebox, with oxygen and moisture levels maintained at less than 0.1 ppm.

The CR2032 coin-type half-cells were assembled with using the above the treated Mg foil or pristine Mg foil as the anode, 0.5 M $\text{Mg}(\text{TFSI})_2/\text{DME}$ as the electrolyte, GF/A Whatman as separator, stainless steel (SS) or Molybdenum (Mo) as the counter electrode, which were abbreviated as BiSn@Mg//SS, BiSn@Mg//Mo or Mg//SS,

Mg//Mo. However, The CR2032 coin-type symmetrical cells were composed of the treated Mg foil or pristine Mg foil anode and cathode, 0.5 M Mg(TFSI)₂/DME electrolyte and GF/A Whatman separator, which is named as BiSn@Mg//BiSn@Mg or Mg//Mg. Then the CR2032 coin-type full-cells were assembled with using the above the treated Mg foil or pristine Mg foil as the anode, 0.5 M Mg(TFSI)₂/DME as the electrolyte, GF/A Whatman as separator and Mo₆S₈ as the cathode, which were abbreviated as BiSn@Mg//Mo₆S₈ or Mg//Mo₆S₈.

Characterization of structure and performance

The morphology of prepared artificial interface layer was examined using an Environmental Scanning Electron Microscope (ESEM, Thermo Fisher Scientific, Quattro S, American) and a Field Emission Transmission Electron Microscope (TEM, Thermo Fisher Scientific, Talos F200S, Czech Republic). And the elemental composition was determined using Energy-Dispersive Spectroscopy (EDS, Thermo Fisher Scientific, Quattro S, American). The X-ray Powder Diffraction (XRD, Panalytical B.V., PANalytical X'Pert Powder, Holland) spectra of the prepared artificial interface layer were accurately recorded by a Rigaku D/MAX2500PC instrument, operated at 40 kV and 30 mA with Cu K α radiation over a diffraction angle range of 20° to 85°, in steps of 1.5° per minute. The surface composition and chemical property of prepared artificial interface layer were further analyzed using multi-functional X-ray Photoelectron Spectroscopy (XPS, Thermo Fisher Scientific ESCALAB250Xi, England). Depth-profiling was performed with Ar⁺ ion sputtering to investigate compositional variations across the interface. Spectra were acquired at three depths: as-prepared surface (0 s), after 100 s etching (~20 nm), and after 200 s etching (~40 nm). To ensure accuracy, all binding energies were calibrated against the carbon peak (C1s) at approximately 284.8 eV, which corresponds to surface adventitious carbon contamination.

Cyclic voltammetry (CV) tests of assembled cells were performed on the CHI-760E electrochemical workstation (Shanghai Chenhua Instruments Co., Ltd.) with a potential range from -1.0 V to 1.0 V and a scan rate of 10 mV s⁻¹, while Tafel curves are derived from cyclic voltammetry (CV) measurements, representing the relationship between current and potential. In this study, symmetric cells were

employed for Tafel analysis. At a fixed scan rate (1 mV s^{-1}) within a defined potential window (-0.2 V to 0.2 V vs. reference), the current response to the applied potential was recorded. The CV data were subsequently converted into Tafel plots ($\log i$ vs. E), from which the exchange current density (i_0) was extracted via linear fitting. The i_0 value reflects the intrinsic kinetics of the electrochemical reaction and serves as a key parameter for assessing electrode activity.

The electrochemical impedance spectroscopy (EIS) tests were implemented with the perturbation voltage set at 10 mV and the frequency range spanning from 10^6 Hz to 10^{-2} Hz . By performing electrochemical impedance spectroscopy (EIS) measurements at various temperatures, interface resistance values under each temperature were extracted through equivalent circuit fitting. The apparent interfacial activation energy was subsequently derived from the Arrhenius equation, which provides a quantitative measure of the kinetic barrier governing the electrochemical reaction, thereby enabling the assessment of its feasibility. In addition, the charge and discharge of different assembled cells were evaluated using the NEWARE battery test system. The current density of symmetric cells Mg//Mg and BiSn@Mg//BiSn@Mg was set to specific values ($0.01 \text{ mA}\cdot\text{cm}^{-2}$, 0.05 mA cm^{-2} , 0.1 mA cm^{-2} , 0.2 mA cm^{-2}) with the controlled charging and discharging times of 1 hour each and a rest period of 30 seconds. The charge and discharge current density of Mg//SS and Mg//Mo₆S₈ cells was 10 mA g^{-1} in the voltage range from 0.2 V to 2.0 V .

CRedit authorship contribution statement

Xiaolong Hou: investigation, conceptualization, writing-original draft, formal analysis. Jingfei Guan: validation and writing – review & editing. Baifei Wu: methodology, formal analysis, validation. Caini Yi: methodology, formal analysis, validation. Shuo Wang: data curation. Guimiao Wang: validation and data curation. Guimiao Wang: data curation. Shuo Wang: data curation. Min Liu: data curation. Meilin Chen: data curation. Liyong Gan: resources and supervision. Danmei Yu: resources, writing – review & editing, supervision, and project administration. Xiaoyuan Zhou: resources, supervision, and funding acquisition.

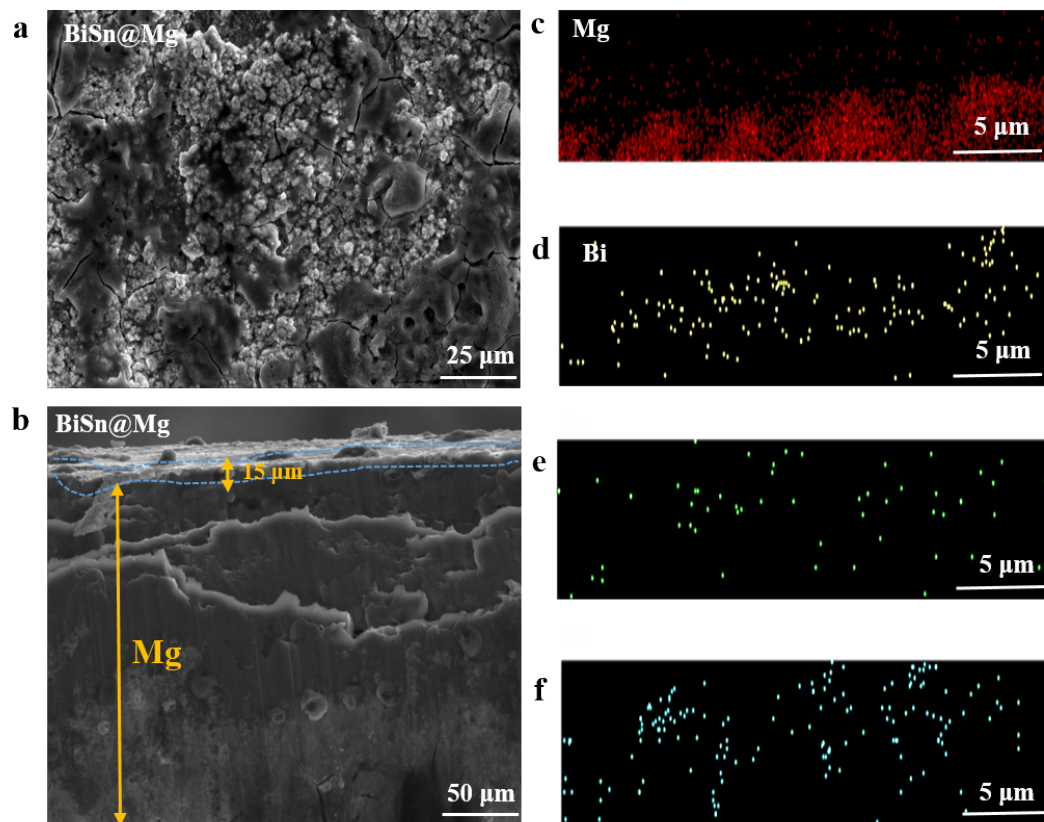


Figure S1. SEM images of (a) top view and (b) cross-sectional view, (c-f) EDS mapping images of Mg, Bi, Sn, and Cl of BiSn@Mg anode after 4000 h charge discharge.

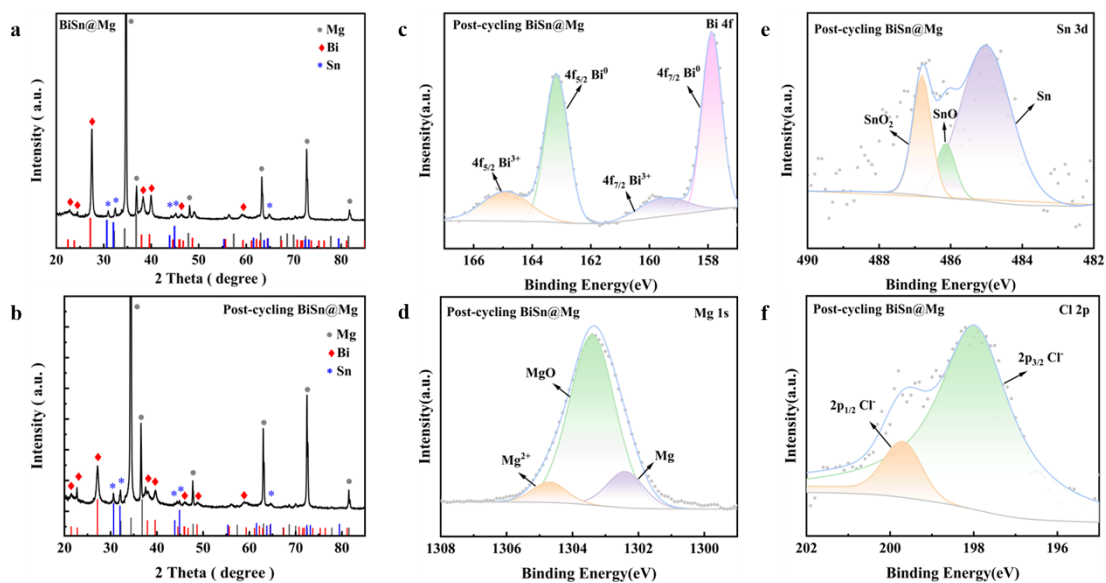


Figure S2. XRD patterns of (a) BiSn@Mg and (b) Post-cycling BiSn@Mg, XPS high resolution spectra of (c) Bi 4f, (d) Mg 1s, (e) Sn 3d and (f) Cl 2p in the Post-cycling BiSn@Mg.

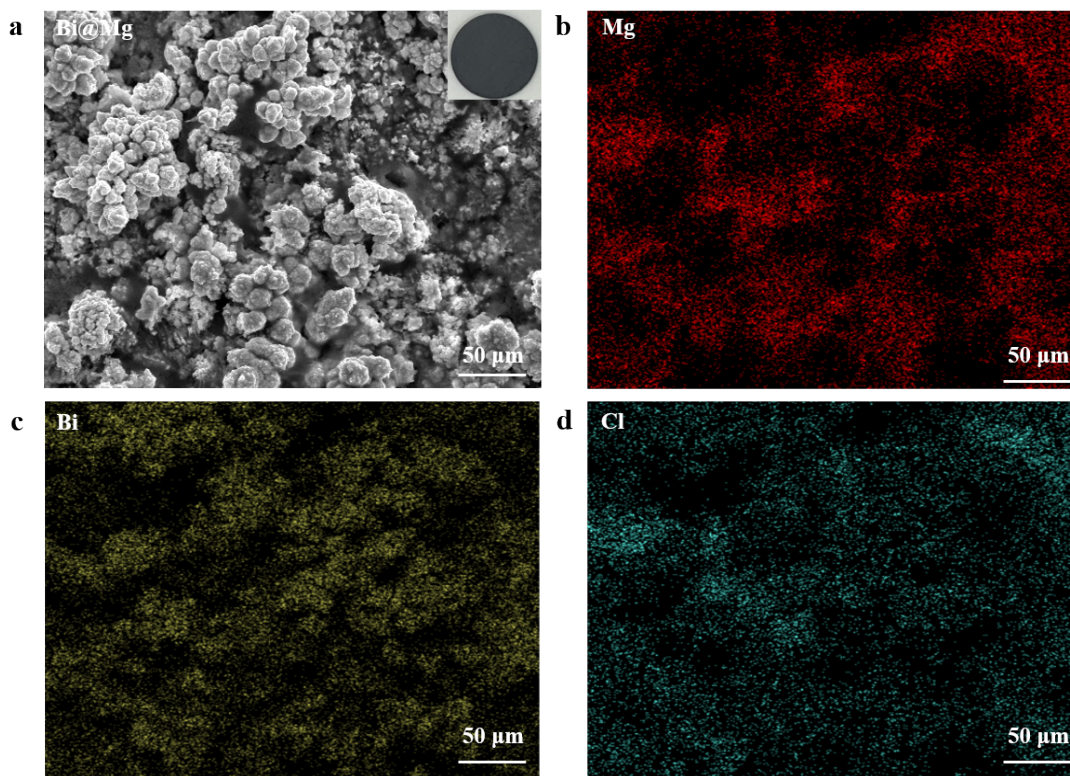


Figure S3. (a) SEM image of top view of Bi@Mg, (b-d) EDS mapping images of Mg, Bi, and Cl element in Bi@Mg.

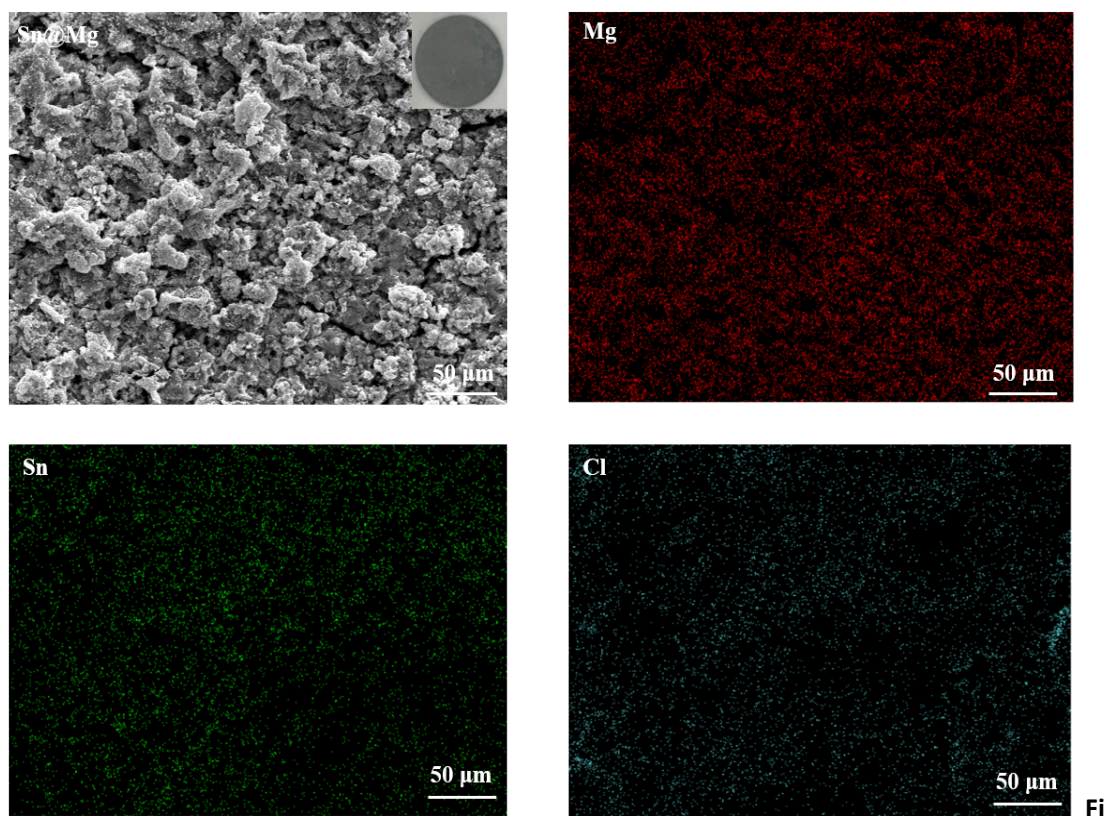


Figure S4. (a) SEM images of top view of Sn@Mg, (b-d) EDS mapping images of Mg, Sn, and Cl element in Sn@Mg.

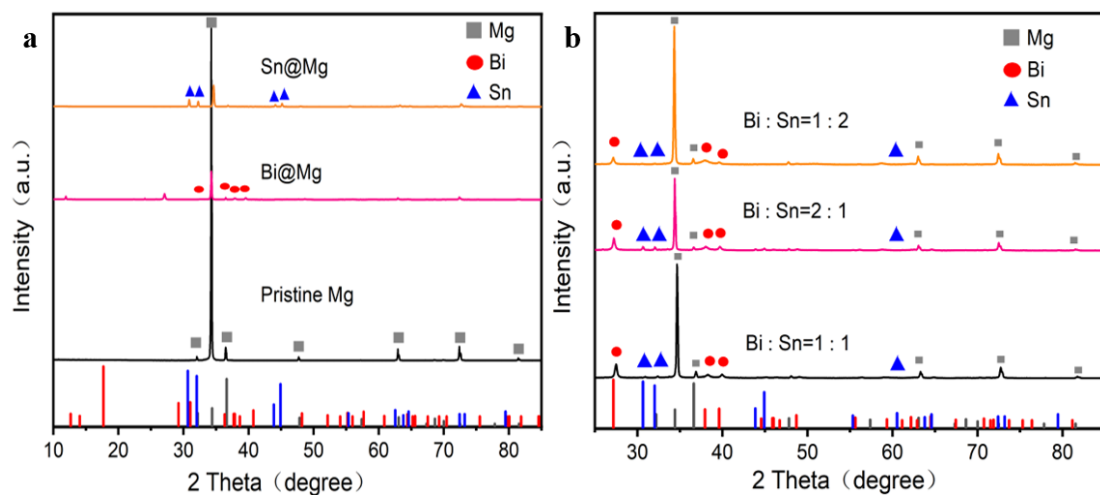


Figure S5. (a) XRD patterns of Bi@Mg, Sn@Mg and pristine Mg electrodes before cycling; (b) XRD patterns of BiSn@Mg electrode.

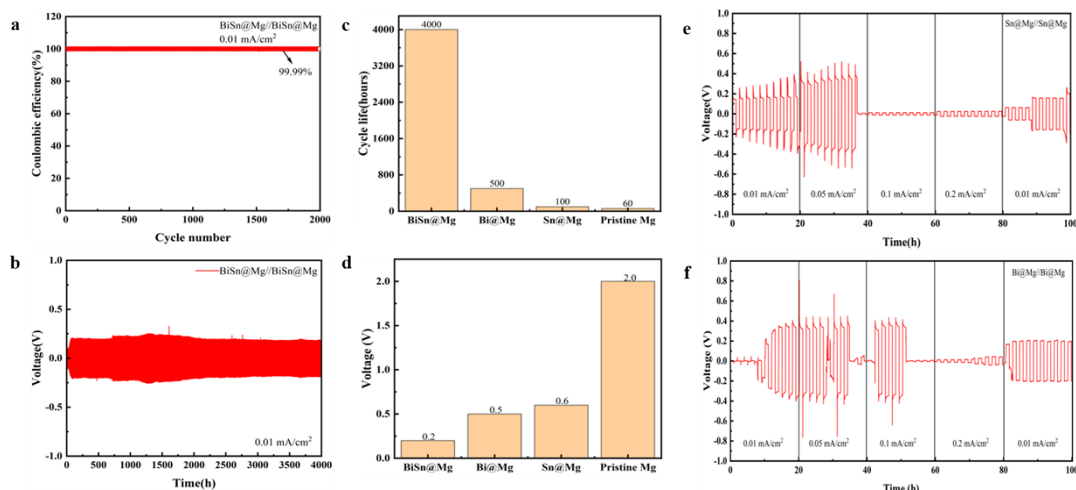


Figure S6. (a) coulombic efficiency and (b) cycling performance of the BiSn@Mg//BiSn@Mg cell at 0.01 mA cm^{-2} ; (c) overpotentials and (d) cycling life of Mg//Mg, Sn@Mg//Sn@Mg, Bi@Mg//Bi@Mg and BiSn@Mg//BiSn@Mg cell; Rate capabilities of (e) Bi@Mg//Bi@Mg and (f) Sn@Mg//Sn@Mg cell.

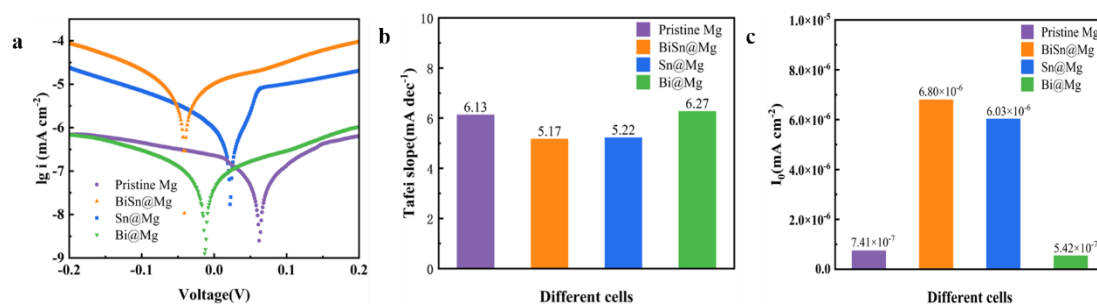


Figure S7. Electrochemical performances of different symmetric cells: (a) Tafel plots, (b) Tafel slope, (c) exchange current density (I_0)

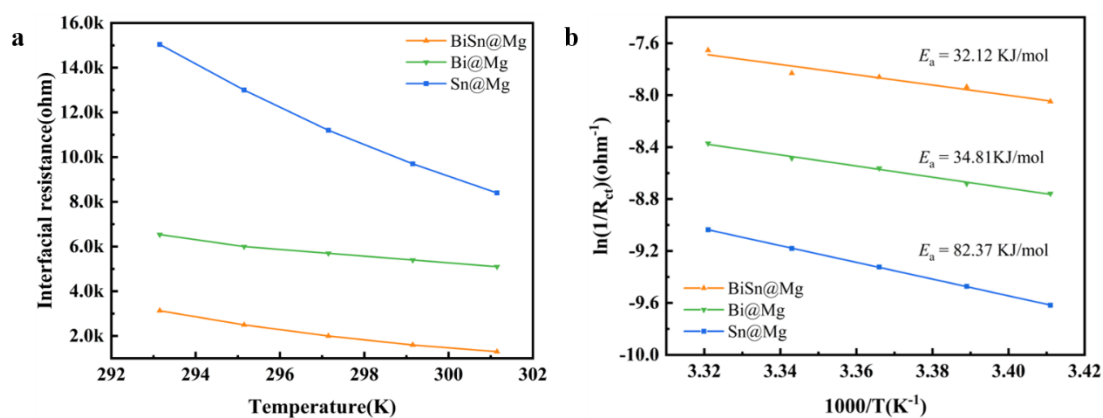


Figure S8. Different symmetric cells (a) the plot of $R_{ct} \sim T$; (b) the plot of $\ln(1/R_{ct}) \sim 1/T$ (solid lines representing Arrhenius fitting).

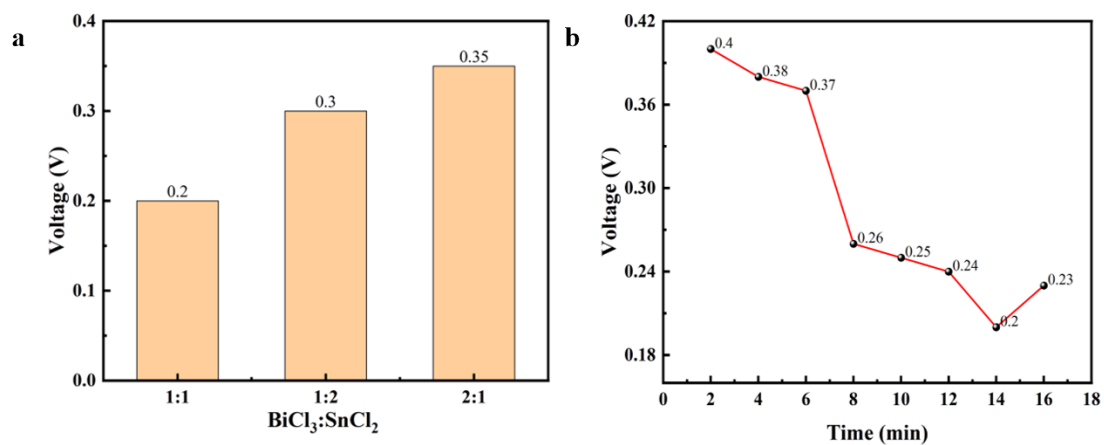


Figure S9. (a) effect of the ratio of BiCl₃ to SnCl₂ metal salts on the overpotential; (b) effect of reaction time on the overpotential.

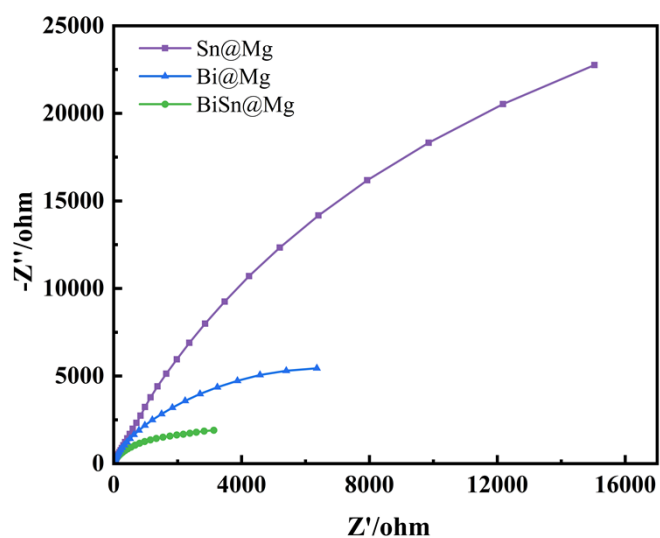


Figure S10. Electrochemical impedance spectroscopy (EIS) of different symmetric cells.

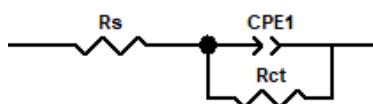


Figure S11. Equivalent circuit diagrams fitted by Nyquist plots (R_s is the electrolyte body resistance, the inherent resistance of the material itself and the contact resistance between various components; R_{ct} is the charge transfer resistance; CPE1 is the constant-phase angle element.)

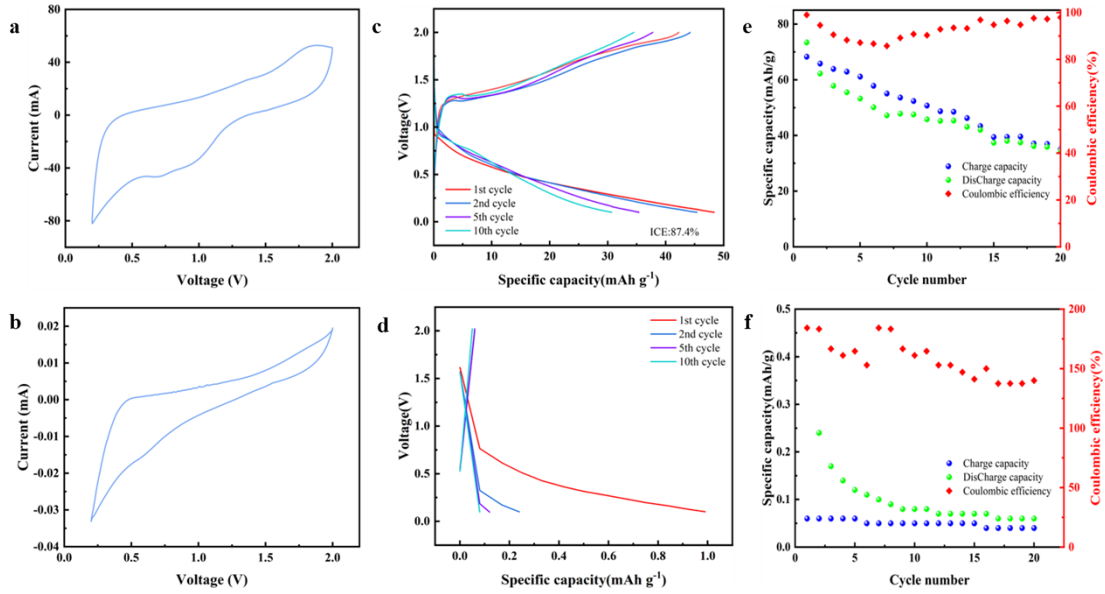


Figure S12. CV curves of (a) BiSn@Mg//Mo₆S₈ and (b) Mg//Mo₆S₈ full cells in Mg(TFSI)₂/DME electrolyte at 1.0 mV s⁻¹; Charge-discharge profiles of (c) BiSn@Mg//Mo₆S₈ and (d) Mg//Mo₆S₈ at 10 mA g⁻¹; Cycling performances of (e) BiSn@Mg//Mo₆S₈ and (f) Mg//Mo₆S₈.

Comparing with conventional Mg-ion batteries using Mo₆S₈, the redox potential of BiSn@Mg//Mo₆S₈ yield an offset due to the effect of the artificial interface and electrolyte.

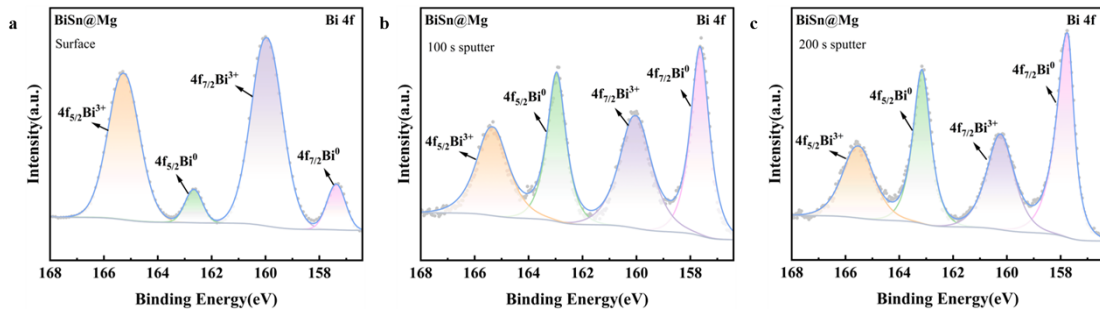


Figure S13. the high-resolution XPS spectra of Bi 4f orbitals in BiSn@Mg at different states (a) As-prepared surface (0 s Ar⁺ sputtering), (b) After 100 s etching (~20 nm depth), (c) After 200 s etching (~40 nm depth).

Table S1. Resistance values of BiSn@Mg//BiSn@Mg and Mg//Mg symmetric cells before charge discharge cycling.

Resistance	R _s /Ω	R _{ct} /kΩ	Error (%)
Pristine Mg	2.248	489.1	5.98
BiSn@Mg	2.153	3.7	0.86